DSC-FLL Based Sensorless Control for Permanent Magnet Synchronous Motor

Yonghong Huang[*]**, Tianyue Tao, Yihang Liu, Kunhua Chen, and FanYang**

Abstract—The $(6k \pm 1)$th harmonics exist in the extended electromotive force estimates due to the influence of the inverter nonlinearities and the flux spatial harmonics in the process of sensorless control of permanent magnet synchronous motor (PMSM), which give rise to the $(6k)$th harmonic in the rotor position estimate. A method of rotor position observation based on the time delay signal cancellation-frequency locked loop (DSC-FLL) is proposed to improve the sensorless control system of PMSM. The equivalent back EMF information is obtained by using the sliding mode observer, and the harmonic component in the specified back EMF observation value is filtered by using the delay signal elimination operator in the two-phase static coordinate system. The frequency locking loop is designed to track the rotor position information online, so as to improve the observation accuracy of the rotor position information. The model of sensorless control system of PMSM based on DSC-FLL is established and compared with the model of sensorless control system of PMSM based on arctangent function. The results show that after adopting the method of rotor position observation based on DSC-FLL, the high harmonic in back EMF is suppressed, the error of rotor position fluctuation observation reduced, and the error of rotation speed observation reduced. The observation accuracy of rotor position information is significantly improved.

1. INTRODUCTION

Permanent magnet synchronous machine (PMSM) has the advantages of high power density, large torque current ratio, wide speed range, and fast dynamic response. It is widely used in electric vehicles, household appliances, compressors, and other fields [1, 2]. The application of sensorless control technology can effectively reduce the volume and cost of the system, increase the reliability of the system, and can be used in harsh environment such as high temperature and high humidity, and has a good application prospect [2]. Sensorless control technology is mainly divided into two categories [3–11]. One type of method is suitable for zero or low speed operation, and it mainly uses the salient pole characteristic of the motor to obtain the position information, including the rotary high frequency signal injection method, pulse vibration high frequency signal injection method, and high frequency square wave signal injection method. The other type is suitable for medium and high speed operation, and the position information is obtained mainly through the reverse electromotive force, namely the model method, including the model reference adaptive method, the sliding mode observer method, the extended Kalman filter method, the effective flux estimation method, etc. The sliding mode observer method has the advantages of strong robustness, good dynamic response, and low sensitivity to motor parameters. It is widely used in PMSM sensorless control.

The concept of extended Back EMF is to reconstruct the PMSM asymmetric voltage model into a symmetric voltage model to obtain the information of rotation speed and rotor position, but the effect of harmonics contained in extended back EMF on the observed results is not considered. Considering

* Corresponding author: Yonghong Huang (hyh@ujs.edu.cn).
The authors are with the School of Electrical and Information Engineering, Jiangsu University, Zhenjiang 212013, China.

the influence of the inverter's nonlinear and magnetic field spatial harmonics, Back EMF contains $(6k \pm 1)$th harmonics, which leads to the $(6k)$th harmonic pulsation in the observed values of rotor position and rotation speed, reducing the observation accuracy of rotor position [12]. In [13], the effect of the nonlinear output of the inverter on the observation of the rotor position was considered, and the resulting observation error of the rotor position was compensated. The method of online parameter identification was adopted to improve the accuracy of the observation of the rotor position, but the effect of the spatial harmonics of the magnetic field on the results was ignored. Therefore, an accurate modeling method of spatial harmonics in magnetic field is proposed [14]. However, this method is dependent on motor parameters and has poor robustness to parameter changes. Literature [15] analyzes the influence of the nonlinear output of the inverter and the spatial harmonics of the magnetic field on the extended Back EMF observation and uses SOGI-FLL method to selectively eliminate the $(6k \pm 1)$th harmonics existing in the Back EMF, so as to improve the observation accuracy. However, SOGI-FLL needs self-adaptive frequency change to generate two-phase orthogonal signals, so the existence of multiple state variables in the structure makes the structure highly nonlinear, resulting in its complex stability analysis.

In the process of PMSM sensorless control, the nonlinearity of inverter and the space harmonics of magnetic field lead to the $6k \pm 1$ times harmonic of Extended Back EMF, which leads to the measurement error of $6k$ rotor position pulsation. In this paper, a rotor position observation method based on delay signal cancellation frequency locked loop (DSC-FLL) is proposed to suppress the pulsation error of rotor position observation and improve the accuracy of rotor position information observation. The equivalent Back EMF information is obtained through the sliding mode observer. After filtering by the delay signal elimination operator [16], the position information of the rotor is tracked by the frequency lock ring [17]. The rotor position observation method based on frequency locking ring of delay signal elimination operator is proposed, which can effectively eliminate the rotor position pulsation error and significantly improve the control performance of PMSM sensorless control system. In this paper, the rotor position pulsation error of PMSM sliding-mode observer method is firstly analyzed, and then the rotor position observation method based on DSC-FLL is designed. Finally, the simulation comparison with the traditional rotor position observation method is carried out to verify the feasibility.

2. ANALYSIS OF PMSM SENSORLESS ROTOR POSITION PULSATION ERROR

2.1. Sensorless Control Strategy of PMSM

The structure block diagram of the sensorless control system of permanent magnet synchronous motor based on DSC-FLL is shown in Figure 1. The system adopts a vector control, which is a double closed-
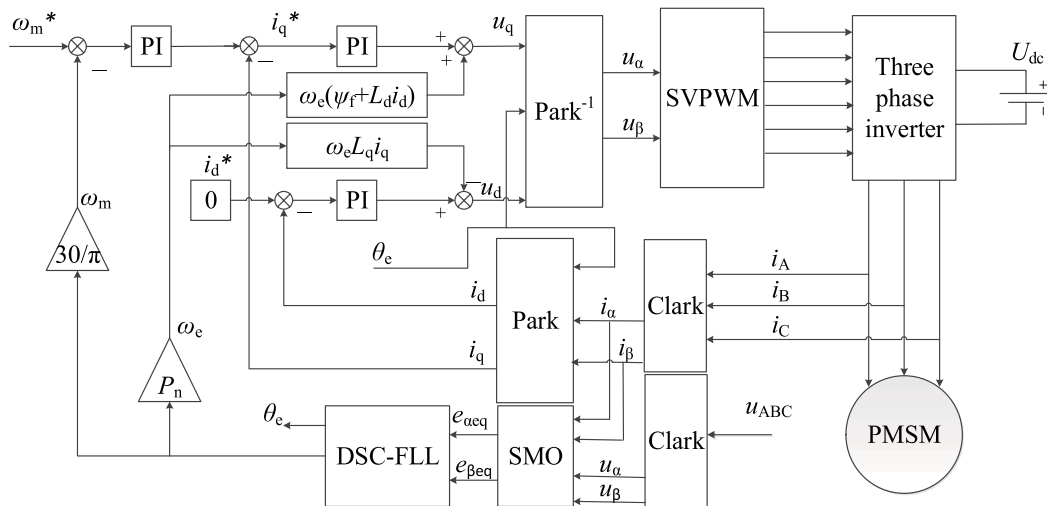
Figure 1. Scheme of sensorless PMSM vector control system.

loop control with an outer loop of speed and an inner loop of current. The equivalent Back EMF information is obtained by using a sliding mode observer. The rotor position is tracked, and the speed information is obtained by using a frequency lock ring. The $(6k\pm1)$th harmonics of the equivalent Back EMF are filtered by the delay signal cancellation operator, and then the position pulsation error of the $(6k)$th rotor is eliminated to improve the performance of the sensorless control system of permanent magnet synchronous motor.

The voltage model of PMSM on the α-β axis can be expressed as

$$\begin{bmatrix} u_\alpha \\ u_\beta \end{bmatrix} = \begin{bmatrix} R + DL_d & \omega_e(L_d - L_q) \\ -\omega_e(L_d - L_q) & R + DL_d \end{bmatrix} \begin{bmatrix} i_\alpha \\ i_\beta \end{bmatrix} + \left[\omega_e\psi_f + (L_d - L_q)(\omega_e i_d - \dot{i}_q)\right] \begin{bmatrix} -\sin\theta_e \\ \cos\theta_e \end{bmatrix} \quad (1)$$

where u_α, u_α is the α-β axial voltage component; i_α, i_α is the α-β axial current component; D is the differential operator; ω_e is the rotor electric angular velocity; θ_e is the electrical angle of the rotor; L_d, L_q is the d-q axis stator inductance; ψ_f is the permanent magnet chain; R is the stator resistance.

Let e be the extended Back EMF(EEMF)

$$e = \begin{bmatrix} e_\alpha \\ e_\beta \end{bmatrix} = \left[\omega_e\psi_f + (L_d - L_q)(\omega_e i_d - \dot{i}_q)\right] \begin{bmatrix} -\sin\theta_e \\ \cos\theta_e \end{bmatrix} \quad (2)$$

where e_α, e_β is the α-β axis extension of the counter electromotive force component, then

$$\begin{bmatrix} u_\alpha \\ u_\beta \end{bmatrix} = \begin{bmatrix} R + DL_d & \omega_e(L_d - L_q) \\ -\omega_e(L_d - L_q) & R + DL_d \end{bmatrix} \begin{bmatrix} i_\alpha \\ i_\beta \end{bmatrix} + \begin{bmatrix} e_\alpha \\ e_\beta \end{bmatrix} \quad (3)$$

According to the above PMSM voltage equation, the sliding mode observer is constructed. Its mathematical model is shown in Equation (4). Figure 2 shows the structural block diagram of the sliding mode observer

$$\begin{cases} \dfrac{d}{dt}\begin{bmatrix} \hat{i}_\alpha \\ \hat{i}_\beta \end{bmatrix} = A \cdot \begin{bmatrix} \hat{i}_\alpha \\ \hat{i}_\beta \end{bmatrix} + \dfrac{1}{L_d}\begin{bmatrix} u_\alpha \\ u_\beta \end{bmatrix} - \dfrac{K}{L_d} \\ e = \begin{bmatrix} e_\alpha \\ e_\beta \end{bmatrix} = \begin{bmatrix} \hat{i}_\alpha - i_\alpha \\ \hat{i}_\beta - i_\beta \end{bmatrix} = 0 \end{cases} \quad (4)$$

where $A = \dfrac{1}{L_d}\begin{bmatrix} -R & -\omega_r(L_d - L_q) \\ \omega_r(L_d - L_q) & -R \end{bmatrix}$; $K = \begin{bmatrix} hsgn(\hat{i}_\alpha - i_\alpha) & hsgn(\hat{i}_\beta - i_\beta) \end{bmatrix}^T$; h is the sliding mode gain, and $sgn(\cdot)$ is the sign function.
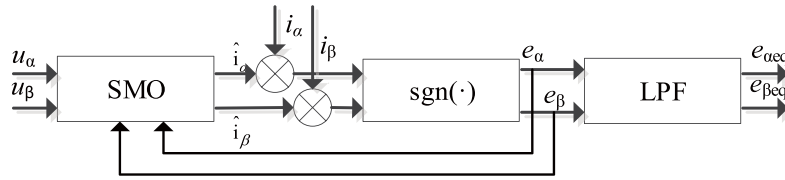
Figure 2. Scheme of SMO.

Then, DSC-FLL is used to obtain the rotor position information. This scheme can quickly track the position change and filter the specified subharmonic, which is beneficial for improving the position observation accuracy.

2.2. Analysis of Rotor Position Fluctuation Error

Considering the effect of the inverter nonlinear and magnetic field space harmonics, $(6k\pm1)$th harmonics exist in the equivalent Back EMF of PMSM, which leads to the $(6k)$th harmonic pulsation in the rotor position and limits the control performance of the system.

Considering the influence of $(6k\pm1)$th harmonic, the model of PMSM extended Back EMF on axis can be rewritten as

$$\begin{bmatrix} u_\alpha \\ u_\beta \end{bmatrix} = \begin{bmatrix} R + DL_d & \omega_e(L_d - L_q) \\ -\omega_e(L_d - L_q) & R + DL_d \end{bmatrix} \begin{bmatrix} i_\alpha \\ i_\beta \end{bmatrix} + e_f + e_h \quad (5)$$

where $e_f = [e_{f\alpha} e_{f\beta}]^T$ is the equivalent Back EMF fundamental component; $e_h = [e_{h\alpha} e_{h\beta}]^T$ is the higher harmonic components. It is expressed in the form of sine wave with amplitude variation value, such as

$$e_h = E_{6k\pm1} \sin\left[(6k \pm 1)\omega_e t + \theta_{6k\pm1}\right] \tag{6}$$

where $E_{6k\pm1}$ is the higher harmonic amplitude; $\theta_{6k\pm1}$ is the initial phase of the higher harmonic.

$(6k \pm 1)$th harmonic in equivalent Back EMF will cause the $(6k)$th harmonic pulsation in rotor position and speed observation, and the sixth harmonic ripple is the most obvious.

3. SPEED AND ROTOR POSITION OBSERVATION BASED ON DSC-FLL

In order to eliminate the error of the $(6k)$th harmonic pulsation of rotor position, the rotor position observation method based on DSC-FLL is adopted, which can selectively eliminate the specified harmonic, eliminate the influence of pulsation error, and improve the observation accuracy.

3.1. Design of DSC Operator

Because of the different rotation angle frequency of each harmonic, the phase difference $\Delta\theta$ of different harmonic turns is different in the same time. When $\Delta\theta=(2k+1)\pi$, $k =0, \pm1, \pm2\ldots$ the average of the two signals is 0. When $\Delta\theta=2k\pi$, $k =0, \pm1, \pm2\ldots$ the two signals coincide, so the specific harmonics can be eliminated by delay operation, and the fundamental wave can be retained, which is called delay signal elimination.

The expression of delay signal elimination operator in time domain is

$$DSC_n\left(v\left(t\right)\right) = \frac{1}{2}\left[v\left(t\right) + v\left(t - T/n\right)\right] \tag{7}$$

where $v(t)$ is the filtered signal; T is the fundamental wave cycle; n is the time delay factor.

Because of the delay element in the delay signal cancellation operator, the phase lag will be introduced into the control loop, which will bring adverse impact on the design of the control loop. In order to avoid this effect, the signal delay cancellation operator can be transformed into α-β coordinate system equivalently.

$$\alpha\beta DSC_n\left(v_{\alpha\beta}\left(t\right)\right) = \frac{1}{2}\left[v_{\alpha\beta}\left(t\right) + e^{j\frac{2\pi}{n}} v_{\alpha\beta}\left(t - T/n\right)\right] \tag{8}$$

where $e^{j2\pi/n}$ is the rotation factor.

The exponential function in Equation (9) is expanded by Euler's formula, and the time domain is realized as

$$\alpha\beta DSC_n = \frac{1}{2}\left\{\begin{bmatrix} v_\alpha\left(t\right) \\ v_\beta\left(t\right) \end{bmatrix} + \begin{bmatrix} \cos(2\pi/n) & -\sin(2\pi/n) \\ \sin(2\pi/n) & \cos(2\pi/n) \end{bmatrix}\begin{bmatrix} v_\alpha\left(t - T/n\right) \\ v_\beta\left(t - T/n\right) \end{bmatrix}\right\} \tag{9}$$

The harmonics of the specified order can be eliminated by setting DSC operators with different n values.

3.2. Frequency Estimation

The basic component of frequency locked loop is frequency estimation.

Under ideal conditions, the frequency of ac signal can be estimated quickly and accurately by solving the derivative of orthogonal signal.

Consider sine input, the calculation formula can be expressed as follows

$$\begin{bmatrix} e_\alpha\left(t\right) \\ e_\beta\left(t\right) \end{bmatrix} = \begin{bmatrix} \sin\left(\omega t + \varphi\right) \\ -\cos\left(\omega t + \varphi\right) \end{bmatrix} \tag{10}$$

According to the characteristics of the trigonometric function relationship, the two-phase signal $\alpha(t)$ and $\beta(t)$ in Equation (11) are used to extract the factor ω by the derivative operation respectively. The calculation formula is

$$\begin{bmatrix} \dot{e}_\alpha\left(t\right) \\ \dot{e}_\beta\left(t\right) \end{bmatrix} = \begin{bmatrix} \omega\cos\left(\omega t + \varphi\right) \\ \omega\sin\left(\omega t + \varphi\right) \end{bmatrix} \tag{11}$$

The sum of squares of the derivatives of $e_\alpha(t)$ and $e_\beta(t)$ was calculated to obtain the angular frequency, namely:

$$(\dot{e}_\alpha(t))^2 + (\dot{e}_\beta(t))^2 = \omega^2 \tag{12}$$

After calculating the square sum of the components on the right side of Equation (12), we can get:

$$\omega = \sqrt{(\dot{e}_\alpha(t))^2 + (\dot{e}_\beta(t))^2} \tag{13}$$

Since there is no ideal differential link, difference is adopted to realize the differential link:

$$\dot{e}_\alpha(k) = \frac{e_\alpha(k) - e_\alpha(k-1)}{T_s} \tag{14}$$

where k is the sampling time; T_s is the sampling period.

Considering difference will introduce error in frequency estimation. Expand Equation (15) in the time domain

$$\dot{e}_\alpha(t) = \frac{1}{T_s} \left\{ \sin(\omega t + \varphi) - \left[\sin(\omega t + \varphi) \left(1 - \frac{\omega^2 T_s^2}{2} \right) + \cos(\omega t + \varphi) \left(\omega T_s - \frac{\omega^3 T_s^2}{6} \right) \right] \right\} \tag{15}$$

So this is going to simplify to

$$\dot{e}_\alpha(t) = \omega \cos(\omega t + \varphi) + \frac{\omega^2 T_s}{2} \sin(\omega t + \varphi) - \frac{\omega^3 T_s^2}{6} \cos(\omega t + \varphi) \tag{16}$$

In the same way, $e_\beta(t)$ can be derived as

$$\dot{e}_\beta(t) = -\omega \sin(\omega t + \varphi) + \frac{\omega^2 T_s}{2} \cos(\omega t + \varphi) + \frac{\omega^3 T_s^2}{6} \sin(\omega t + \varphi) \tag{17}$$

By substituting Equations (16) and (17) into Equation (12), the following equation can be obtained as

$$(\dot{e}_\alpha(t))^2 + (\dot{e}_\beta(t))^2 = \omega^2 - \frac{\omega^4 T_s^2}{12} + \frac{\omega^6 T_s^4}{36} \approx \omega^2 - \frac{\omega^4 T_s^2}{12}, \frac{\omega^6 T_s^4}{36} \ll \frac{\omega^4 T_s^2}{12} \tag{18}$$

As mentioned in Equation (18), the error caused by the introduction of difference link shall be compensated by adding $\omega^4 T_s^2/12$ to the frequency estimation.

3.3. Design of DSC-FLL

The frequency-locked loop can be used to track voltage phase quickly and has better dynamic performance. More stable frequency information is used as the feedback controller to avoid the phase controller with more frequent fluctuation.

Figure 3 is the block diagram of frequency and Angle estimation based on DSC-FLL.
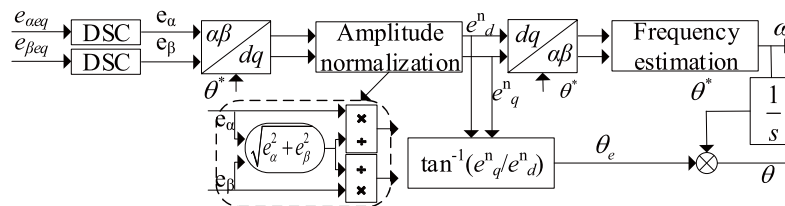
Figure 3. Frequency and phase estimation based on DSC-FLL.

In Figure 3, $e_\alpha(t)$, $e_\beta(t)$ are transformed by Park into

$$\begin{bmatrix} e_d(t) \\ e_q(t) \end{bmatrix} = T_{dq} \begin{bmatrix} e_\alpha(t) \\ e_\beta(t) \end{bmatrix} = E \begin{bmatrix} \cos(\Delta\omega t) \\ \sin(\Delta\omega t) \end{bmatrix} \tag{19}$$

where E is the amplitude of Back EMF; ω is the given angular frequency; ω_e is the output angular frequency, and T_{dq} can be derived as

$$T_{dq} = \left[\begin{array}{cc} \cos\theta^* & -\sin\theta^* \\ \sin\theta^* & \cos\theta^* \end{array} \right] \tag{20}$$

$$\Delta\omega = \omega - \omega_e \tag{21}$$

After the amplitude is normalized, it is obtained by the inverse Park transformation.

$$\left[\begin{array}{c} e_\alpha^n(t) \\ e_\beta^n(t) \end{array} \right] = T_{dq}^{-1} \left[\begin{array}{c} e_d^n(t) \\ e_q^n(t) \end{array} \right] = \left[\begin{array}{c} \cos\left[(\Delta\omega + \omega_e)\,t\right] \\ \sin\left[(\Delta\omega + \omega_e)\,t\right] \end{array} \right] \tag{22}$$

The frequency estimation method in Section 3.2 can be used to estimate the frequency of Equation (22):

$$\omega = \sqrt{(\dot{e}_\alpha^n(t))^2 + \left(\dot{e}_\beta^n(t)\right)^2} = \Delta\omega + \omega_e \tag{23}$$

According to Equation (11), it can be seen that the actual position angle of the rotor consists of two parts: the initial angle and the product of the angular frequency and time.

In Figure 3, the angle θ^* obtained by integrating the output angular frequency of frequency estimation is the product of angular frequency and time. The initial angle can be calculated by the d-q axis voltage component after amplitude normalization.

$$\theta_0 = \arctan\left(\frac{e_q^n(t)}{e_d^n(t)}\right) \tag{24}$$

Then the actual position angle of the output rotor of the frequency lock ring is

$$\theta = \theta_0 + \theta^* \tag{25}$$

4. VERIFICATION AND ANALYSIS OF SIMULATION RESULTS

In order to verify the correctness of the proposed algorithm, a simulation model of rotor position observation method based on DSC-FLL was established in Matlab/Simulink simulation environment. The PI parameters of each loop in the model in Figure 1 have been given, and the speed loop KP = 0.1, KI = 1; the current loop KP = L*1100, KI = R*1100; the sliding mode gain is 200; The expected bandwidth of the LPF of the sliding mode observer is 20000. PMSM parameters are shown in Table 1.

Table 1. Parameters of the PMSM.

| Motor parameters	value	Motor parameters	value
Rated power /kW	1.1	Polar logarithm/p_n	4
Permanent magnet flux linkage /Wb	0.175	Moment of inertia /(kg· m^2)	0.0026
DQ axis inductance /mH	8.5	Resistance /Ω	2.875

Figure 4 shows the observed results of Back EMF under the condition of $600\,\mathrm{r/min}$. Figures 4(a) and (c) show the observation results of the counter electromotive force after using the traditional rotor position observation method and the rotor position observation method based on DSC-FLL respectively. It can be seen from the results that the waveform of the counter electromotive force is smoother after using the rotor position observation method based on DSC-FLL. Figures 4(b) and 4(d) show the FFT analysis results after the traditional rotor position observation method and the rotor position observation method based on DSC-FLL, respectively. It can be seen from the results that the 5th and 7th harmonics in the observed value of the reverse electric potential can be effectively filtered after the rotor position observation method based on DSC-FLL. It can be seen that DSC-FLL can effectively filter the 5th and 7th harmonics in the back EMF.
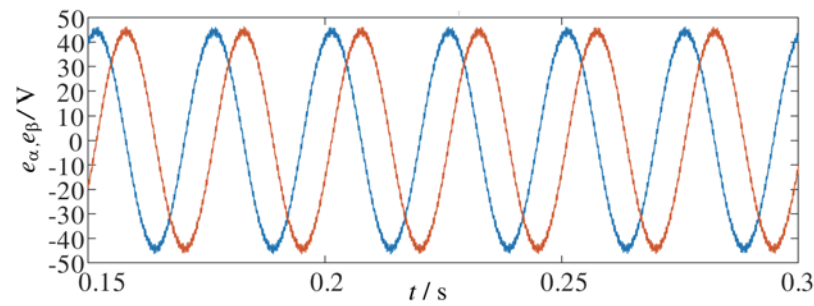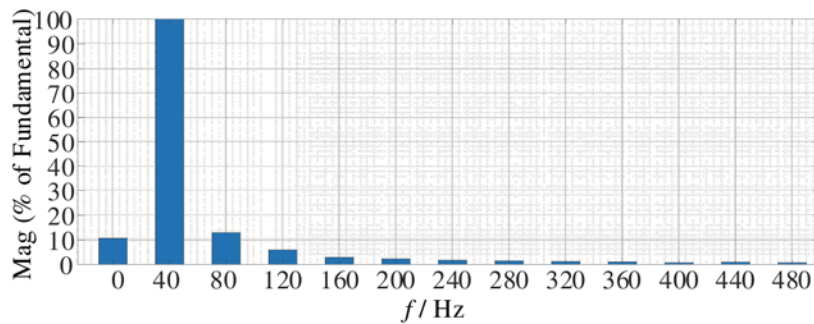
(a) Back EMF after using traditional rotor position observation method
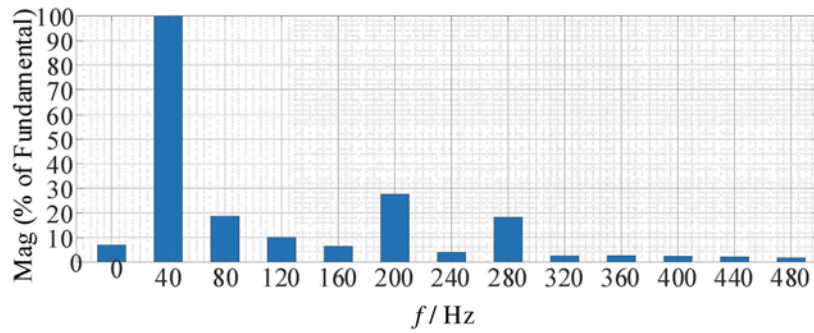
(b) FFT analysis of the back EMF using traditional rotor position observation method
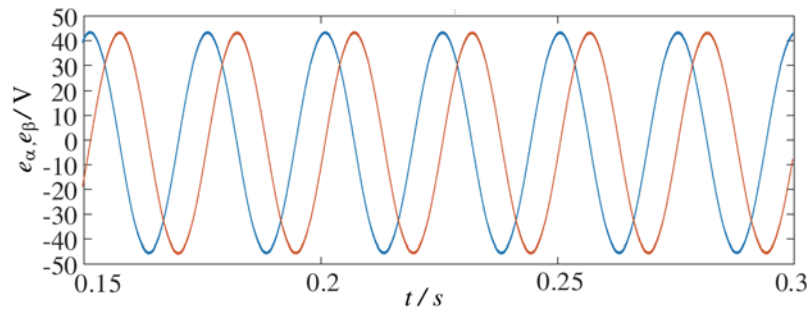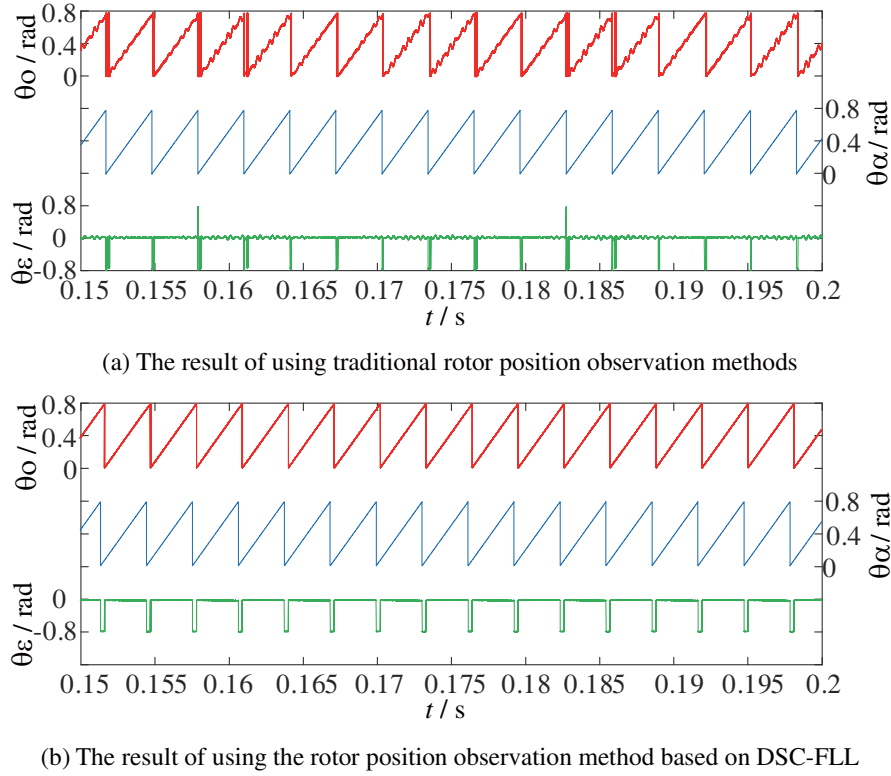

(c) Back EMF after using the rotor position observation method based on DSC-FLL

(d) FFT analysis of the back EMF using rotor position observation method based on DSC-FLL

Figure 4. Back EMF estimates and the FFT analysis.

Figure 5 shows the observed position (θo), actual position (θa), and position error (θe) results under the condition of $600\,\mathrm{r/min}$. Figures 5(a) and 5(b) show the observation results after using the traditional rotor position observation method and the rotor position observation method based on DSC-FLL. The observation position, actual position, and position observation error are shown from top to bottom.

(a) The result of using traditional rotor position observation methods

(b) The result of using the rotor position observation method based on DSC-FLL
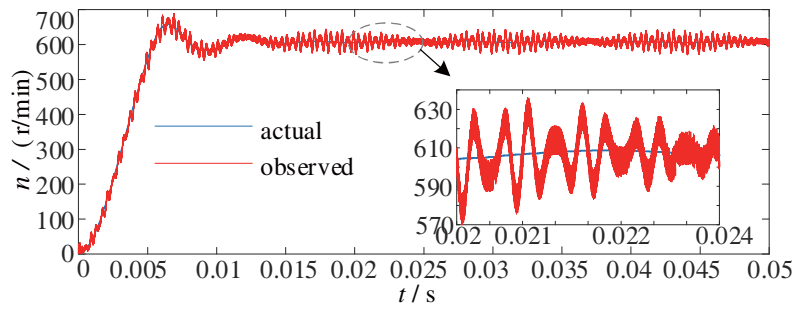
Figure 5. Waveforms with estimated position, actual position and estimation error.

It can be seen from the results that after using the rotor position observation method based on DSC-FLL, the amplitude of position observation error pulsation decreases from 0.112 rad to 0.008 rad; the rotor position observation value becomes smoother; the rotor position observation accuracy is effectively improved.

Figure 6 shows the estimation error results of observed speed, actual speed, and rotation speed under the condition of 600 r/min. Figures 6(a) and 6(c) show the observed speed and actual speed observation results after using the traditional rotor position observation method and the rotor position observation method based on DSC-FLL. It can be seen from the results that the observation curve and actual curve can be better fitted. Figures 6(b) and 6(d) are the observation results of the speed estimation error after using the traditional rotor position observation method and the rotor position observation method based on DSC-FLL. It can be seen from the results that after using the rotor position observation method based on DSC-FLL. The fluctuation amplitude of rotor speed observation error is reduced from 30 r/min to 9 r/min; the rotor speed fluctuation is reduced; the rotor speed observation accuracy is effectively improved.

Figure 7 shows the dynamic performance results when the rotor position observation method based on arctangent function and the rotor position observation method based on DSC-FLL are used, and the motor speed increases from 400 r/min to 700 r/min and then drops to 400 r/min. Figures 7(a) and 7(b) show the observation results after using the traditional rotor position observation method and the rotor position observation method based on DSC-FLL, respectively, and the observation speed, speed observation error, and position observation error are in order from top to bottom. It can be seen from the results that the fluctuation amplitude of speed observation error is reduced from 30 r/min to 9 r/min, and the fluctuation amplitude of position observation error is reduced from 0.112 rad to 0.008 rad, which shows that the dynamic control performance is better.

It can be found that after adopting the rotor position observation method based on DSC-FLL, the $(6k \pm 1)$th harmonic in the back EMF observed of the motor is significantly suppressed. The observed position error is significantly reduced, and the position observation accuracy is significantly improved.
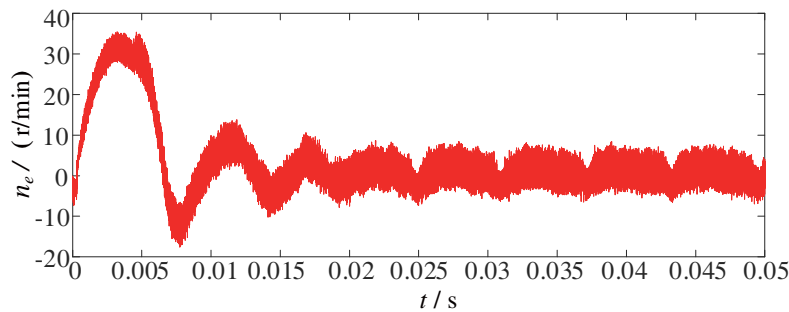
(a) Observation speed and actual speed after using traditional rotor position observation method
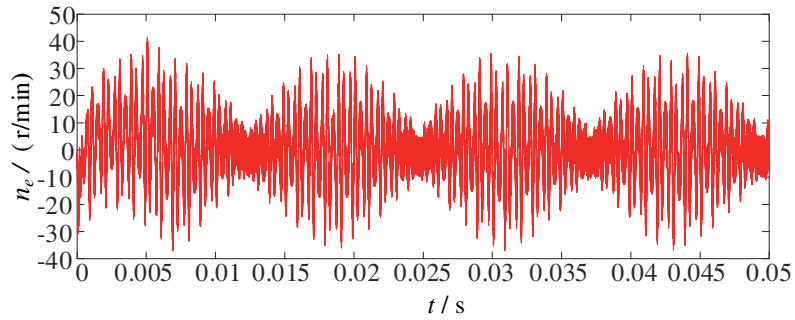
(b) Observation error after using traditional rotor position observation method
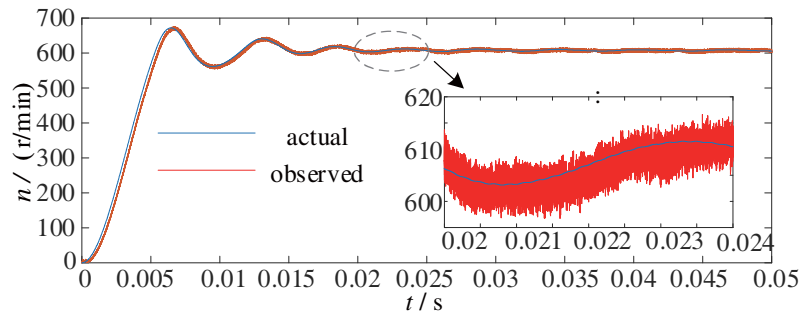

(c) Observed speed and actual speed after using the rotor position observation method based on DSC-FLL

(d) Observation error of rotor position observation method based on DSC-FLL

Figure 6. Waveforms with estimated speed, actual speed and estimation error.

The rotor velocity observation error is significantly reduced, and the rotor position observation accuracy is significantly improved, indicating that DSC-FLL has good observation performance in both steady state and dynamic state.

(a) After using traditional rotor position observation method

(b) After using the rotor position observation method based on DSC-FLL
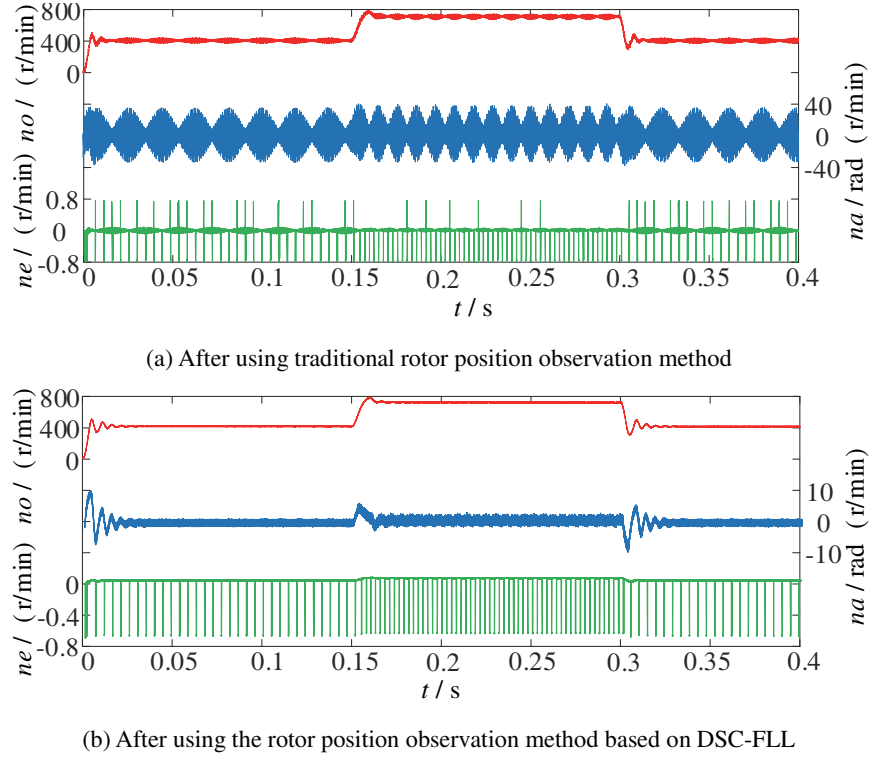
Figure 7. Experimental results with speed variations.

5. CONCLUSION

In this paper, a sensorless control method for PMSM based on DSC-FLL is proposed. The sliding-mode observer of back EMF is used to obtain the equivalent back EMF information, and the rotor position information is tracked by the FLL. Considering the effect of the inverter nonlinear and the spatial harmonics of the rotor magnetic field, the $(6k \pm 1)$th harmonics in the equivalent back EMF are filtered by the DSC operator, so as to eliminate the $(6k)$th pulsation error of the rotor position observation and improve the observation accuracy. The model of sensorless control system of PMSM based on DSC-FLL was established and compared with the traditional PMSM sensorless control system model. It was found that after adopting the rotor position observation method based on DSC-FLL, the $(6k \pm 1)$th harmonic in the counter potential was suppressed, the rotor position pulsation observation error reduced, and the rotation speed observation error reduced. It is shown that the proposed DSC operator can effectively reduce the rotor position observation pulsation error; the convergence speed is faster; the steady-state and dynamic control effect is better.

ACKNOWLEDGMENT

REFERENCES

1. Wang, G., R. Yang, Y. Yu, et al., "Position sensorless control for interior permanent magnet synchronous motor," *Proceedings of the CSEE*, Vol. 30, No. 30, 93–98, 2010.

2. Liu, J., F. Xiao, Y. Shen, et al., "Position-sensorless control technology of permanent-magnet synchronous motor-a review," *Transactions of China Electrotechnical Society*, Vol. 32, No. 16, 76–88, 2017.

3. Wang, G., G. Zhang, X. Gui, et al., "Hybrid sensorless control strategy for permanent magnet synchronous motors," *Proceedings of the CSEE*, Vol. 32, No. 24, 103–109, 2012.

4. Yu, C. Y., J. Tamura, D. D. Reigosa, et al., "Positionself-sensing evaluation of a FI-IPMSM based on high-frequency signal injection methods," *IEEE Transactions on Industry Applications*, Vol. 49, No. 2, 880–888, 2013.

5. Li, J., B. Zhou, B. Liu, et al., "A novel starting strategy of sensorless control for surface mounted permanent magnet synchronous machines," *Proceedings of the CSEE*, Vol. 36, No. 9, 2513–2520, 2016.

6. Zhang, G., G. Wang, D. Xu, et al., "Adaptive notch filter based rotor position estimation for interior permanent magnet synchronous motors," *Proceedings of the CSEE*, Vol. 36, No. 9, 2521–2527, 2016.

7. Bolognani, S., L. Tubiana, and M. Zigliotto, "Extended Kalman filter tuning in sensorless PMSM drives," *IEEE Transactions on Industry Applications*, Vol. 39, No. 6, 1741–1747, 2003.

8. Zhang, Q. and D. Li, "Sensorless vector control of PMSM Based on adaptive second order sliding mode observer with parameter identification ," *Control and decision making*, Vol. 34, No. 7, 1385–1393, 2019.

9. Sarikhani, A. and O. A. Mohammed, "Sensorless control of PM synchronous machines by physics-based EMF observer ," *IEEE Transactions on Energy Conversion*, Vol. 27, No. 4, 1009–1017, 2012.

10. Wang, G., R. Yang, and D. Xu, "DSP-based control of sensorless IPMSM drives for wide-speed-range operation ," *IEEE Transactions on Industrial Electronics*, Vol. 60, No. 2, 720–727, 2013.

11. Lee, J., J. Hong, K. Nam, et al., "Sensorless control of surface-mount permanent-magnet synchronous motors based on a nonlinear observer," *IEEE Transactions on Power Electronics*, Vol. 25, No. 2, 290–297, 2010.

12. Chen, Z., M. Tomita, S. Doki, et al., "An extended electromotive force model for sensorless control of interior permanent-magnet synchronous motors," *IEEE Transactions on Industrial Electronics*, Vol. 50, No. 2, 288–295, 2003.

13. Inoue, Y., K. Yamada, S. Morimoto, et al., "Effectiveness of voltage error compensation and parameter identification for model-based sensorless control of IPMSM," *IEEE Transactions on Industry Applications*, Vol. 45, No. 1, 213–221, 2009.

14. Jung, S. H., H. Kobayashi, S. Doki, et al., "An improvement of sensorless control performance by a mathematical modelling method of spatial harmonics for a SynRM," *International Power Electronics Conference (IPEC)*, 2110–2015, Sapporo, Japan, 2010.

15. Wang, G., L. Ding, Z. Li, et al., "Enhanced position observer using second-order generalized integrator for sensorless interior permanent magnet synchronous motor drives," *IEEE Transactions on Energy Conversion*, Vol. 29, No. 2, 486–495, 2014.

16. Wu, H., D. Yang, and X. Ruan, "Phase-locked loop based on cascaded delayed signal cancellation for distorted grid," *Trans of China Electro-technical Society*, Vol. 29, No. 8, 255–264, 2014.

17. Zou, B., H. Li, Y. Li, et al., "Phase-locked technology based on novel three-phase frequency-locked loop," *Proceedings of the CSU-EPSA*, Vol. 31, No. 3, 76–82, 2019.